

Infrared Cooling Rate Calculations in Operational General Circulation Models: Comparisons with Benchmark Computations

S. B. FELLS,^{1,2} J. T. KIEHL,³ A. A. LACIS,⁴ AND M. D. SCHWARZKOPF²

As part of the Intercomparison of Radiation Codes in Climate Models (ICRCCM) project, careful comparisons of the performance of a large number of radiation codes were carried out, and the results compared with those of benchmark calculations. In this paper, we document the performance of a number of parameterized models which have been heavily used in climate and numerical prediction research at three institutions: Geophysical Fluid Dynamics Laboratory (GFDL), National Center for Atmospheric Research (NCAR), and Goddard Institute for Space Studies (GISS).

1. INTRODUCTION

One of the important goals of the World Meteorological Organization (WMO)-sponsored Intercomparison of Radiation Codes in Climate Models (ICRCCM) project was the careful documentation of the performance of radiation codes which have been used in operational climate and numerical weather prediction models. To this end, extensive statistical summaries have been compiled which give a précis of the most important fluxes calculated by various models for a large number of standard ICRCCM cases. The article by *Ellingson et al.* [this issue] discusses some of these results. In addition to fluxes at the top and bottom of the atmosphere, however, the infrared cooling rates themselves play an important part in determining the climatology of the model atmosphere. It has been suggested, for example, that the "cold bias" observed in the upper troposphere of a number of climate models might be due to deficiencies in the treatment of radiative cooling there. In addition to such direct climatological effects, there is some evidence [*Ramanathan et al.*, 1983] that subtle changes in the treatment of radiative transfer can also have important effects on the model dynamics.

It is therefore desirable to have available a rather detailed discussion of the cooling rates as well as of the fluxes calculated by radiative models used in a number of operational general circulation models, together with a brief description of their construction and shortcomings. It is the purpose of this paper to provide these.

Radiation models discussed in this study have been used over a period of time in general circulation models (GCMs), and there exists a body of literature describing applications of these GCMs to diverse climate problems. We are chiefly interested in documenting the behavior, even if less accurate, of older "production" GCMs including these radiative models, rather than in evaluating the performance of more detailed "off-line" models or newer models, which are currently under development.

The models to be described are listed in Table 1, along with their chief architects and period of active use. It is interesting to notice that in several instances, more than one distinct radiation code has been in use at a given institution. We believe that the models discussed cover a significant fraction of the GCM climate and numerical weather prediction literature of the past decade.

It is important to recognize that very often radiative algorithms undergo revision during their working lifetime. While this is often due to a desire to include new physics or to increase computational speed, it is also occasionally due to the discovery of a code error. In the descriptions which follow, a conscientious effort has been made to discuss such changes if they make a significant difference in the performance of the code.

The organization of the paper is extremely simple. In the next section, we briefly describe the standard ICRCCM cases that all of the models use. In subsequent sections, the performance of each of the models is documented.

We have tried to keep the description uniform across the various models. Within each model section, the level structure is first summarized, and a very brief description of the particular model given, along with a short summary of the major publications in which it has appeared. The cooling rate and flux results are then presented (on the actual model levels), along with the corresponding values obtained from line-by-line benchmark calculations carried out in the course of the ICRCCM study. Finally, there is a brief discussion of these results.

2. DESCRIPTION OF ICRCCM CASES AND THE LINE-BY-LINE MODEL

From the original 37 standard cases of the ICRCCM protocol for clear-sky longwave calculations, we shall present cooling rates and fluxes for three: 25, 27, and 33 (tropical (T), mid-latitude summer (MLS), and subarctic winter (SAW), respectively). The temperature, water vapor, and ozone mixing ratio profiles for these cases are given by *McClatchey et al.* [1972]. Carbon dioxide is assumed to be uniformly mixed at 300 ppmv.

In addition to these three cases, we shall also present selected flux difference results using cases 26, 28, and 36. These are the same soundings as the previous three, but with 600 ppmv CO₂. In most cases, it is the change in the net flux at the tropopause that will be of greatest interest, since it is most directly related to the change in tropospheric temperature in GCMs.

¹Deceased October 22, 1989.

²Geophysical Fluid Dynamics Laboratory, Princeton, New Jersey.

³National Center for Atmospheric Research, Boulder, Colorado.

⁴NASA Goddard Institute for Space Studies, New York.

Copyright 1991 by the American Geophysical Union.

Paper number 91JD00516,
0148-0227/91/91JD-00516\$05.00

TABLE 1. Description of Models Employed in Comparison

Institute	Model	Chief Architects	Period of Use
GFDL	I	Manabe and Stone	1970–1984
	II		1984–1986
	III		1986–present
	I II	Fels and Schwarzkopf	1975–present 1986–present
NCAR	CCM0	Ramanathan Kiehl, Ramanathan, and Briegleb	1983–1987
	CCM1		1987–present
GISS	Model II	Lacis and Oinas	1983–present

The benchmark calculations were performed using the Geophysical Fluid Dynamics Laboratory (GFDL) line-by-line (LBL) model, which is a distant descendant of the code described by Drayson [1973]. Full details of these LBL calculations are described by Schwarzkopf and Fels [this issue]. The calculations, which fully resolve even the centers of Voigt lines, include a frequency range extending from 0 to either 2200 or 3000 cm^{-1} . In making comparisons with the parameterized calculations, the LBL values are given over the same frequency range as that used in the parameterizations. Cooling rate comparisons are, in any case, quite insensitive to the choice of the upper bound, provided the water vapor rotation band is fully included. Spectral data are taken from the 1980 Air Force Geophysics Laboratory (AFGL) compilation [Rothman, 1981]. Water vapor and ozone line absorption profiles are cut off at 10 cm^{-1} , and carbon dioxide lines at 3 cm^{-1} . The water vapor continuum is included with coefficients taken from Roberts *et al.* [1976]. The vertical grid has 123 levels between the ground and about 90 km. Temperature profiles for this grid are generated using the algorithm described by Fels [1986], while the water vapor and ozone mixing ratios are obtained by interpolation from the tables in McClatchey *et al.* [1972]. Further details on the vertical grid and on the derivation of the vertical profiles are found in Appendix A of Schwarzkopf and Fels [this issue].

In the following sections, these LBL results are compared with those obtained with the parameterized models included in Table 1. In general, the errors made by the GCM calculations are due to (1) the lack of spectral resolution (and to other physical approximations), and (2) the lack of vertical resolution. In almost all of the results to be discussed, the errors include contributions from both sources. To evaluate the significance of errors in the parameterized models due to vertical resolution, we include, in section 6, a discussion of the effect of increased vertical resolution on the National Center for Atmospheric Research Community Climate Model, version 1 (NCAR CCM1) model results; a similar discussion on the Fels-Schwarzkopf model is found in Schwarzkopf and Fels [this issue]. Although differences are observed in fluxes at the tropopause and the top, and in upper tropospheric cooling rates, the overall conclusions of this paper are not significantly affected.

Cooling rate results from the LBL model are presented as continuous solid lines in all figures, a representation consistent with the high vertical resolution employed. Results from parameterized models are displayed as averages over the coarse vertical layers used in these models.

3. GFDL MODEL RESULTS (MANABE-STONE, VERSIONS I, II, AND III)

Model Description and Usage

The Manabe-Stone algorithm has been the standard radiative transfer module used for climate modeling at GFDL since 1970. It is primarily a tropospheric model; most research with it employs a nine-level σ -vertical coordinate grid, with temperatures, mixing ratios, and cooling rates carried at sigma levels of 0.025, 0.095, 0.205, 0.350, 0.515, 0.680, 0.830, 0.940, and 0.990. Water vapor is treated using the 19 band random-model formulation of Rodgers and Walshaw [1966]. All of the models discussed in this section use the spectral data given in that paper. Carbon dioxide transmission functions are calculated by interpolation from tables of absorptivities whose arguments are pressure, absorber amount and temperature. The tabulated values have been obtained from LBL calculations for homogeneous paths performed by R. Drayson. The ozone 9.6- μm band is included by use of the one-band Malkmus formulation of Rodgers [1968]. The frequency range extends from 0 to 2200 cm^{-1} .

There have been a number of changes during the time in which the code has been in use. The most important of these is the replacement of the *p*-type water continuum (version I) of Rodgers and Walshaw [1966] by the *e*-type continuum of Bignell [1970]. This modification was made in 1984, but due to a code error, the strength of the continuum was underestimated by 62% (version II). Papers that use this code have been indicated below by an asterisk. In 1985, this error was corrected and continuum coefficients were taken from Roberts *et al.* [1976] (version III); papers incorporating this correction are shown with a double asterisk. A detailed description of the original model construction is given by Stone and Manabe [1968].

This radiation code has been used in all of the climate simulation and increased carbon dioxide sensitivity studies carried out at GFDL by Manabe and collaborators since 1970. These include the effect of increased CO_2 in an annually averaged GCM [Manabe and Wetherald, 1975], in a seasonal model [Wetherald and Manabe, 1981; Manabe and Wetherald, 1987*], in a global model with a mixed layer [Manabe and Stouffer, 1979, 1980], and in a combined ocean-atmosphere model [Bryan *et al.*, 1982, 1988**]. In view of the emphasis on this problem, we shall pay special attention in our discussion of the results to those that involve sensitivity to doubled carbon dioxide. In addition, the code has been used in studies of interannual climate variability, El Niño-Southern Oscillation (ENSO), and of paleoclimate [Manabe and Broccoli, 1985; Broccoli and Manabe, 1987].

Cooling Rate Results

Cooling rates computed using the parameterized and LBL algorithms for the T, MLS, and SAW profiles are displayed in Figures 1a-1c (for version I), in Figures 2a-2c (for version II), and in Figures 3a-3c (for version III). Comparison of the results for version I, which had a simple *p*-type continuum, with those of the other versions indicates clearly that the crude treatment of the continuum leads to a significant underestimate of the lower tropospheric cooling rates in the water-rich T and MLS cases. The excessive cooling near 350 mbar has been explained by Ramanathan and Downey [1986] as being due to the use

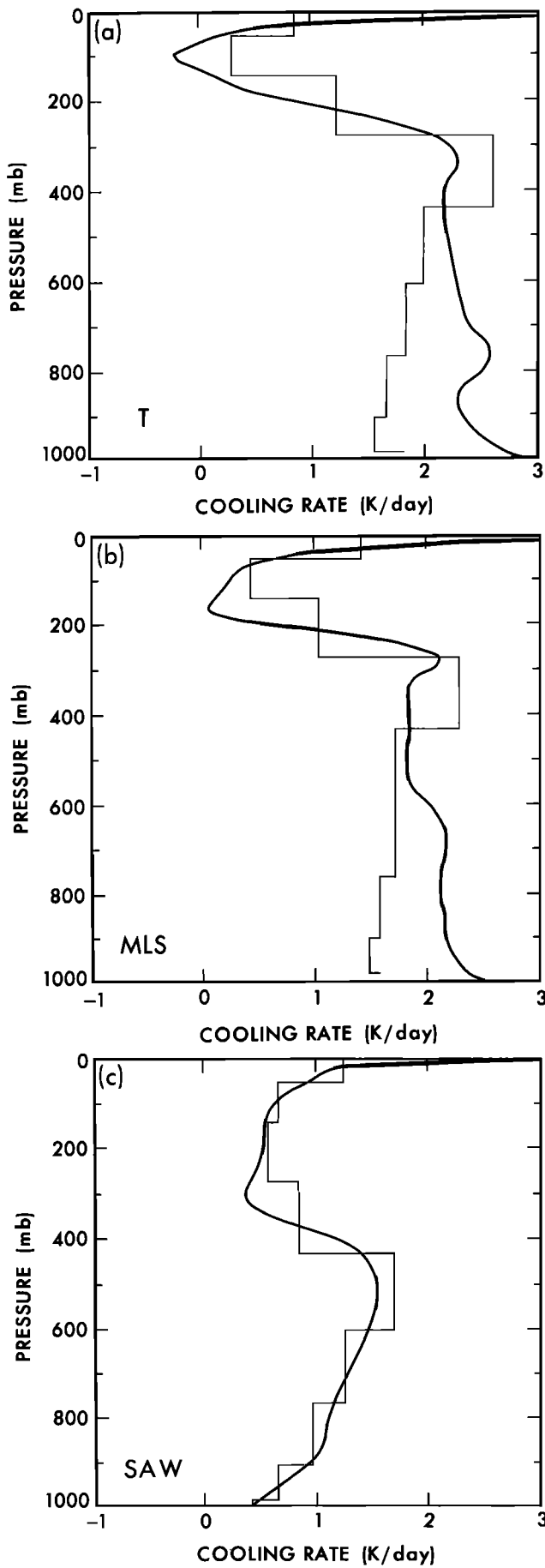


Fig. 1. Cooling rate profiles ($K d^{-1}$) from version I of the GFDL Manabe-Stone model for (a) tropical, (b) mid-latitude summer, and (c) subarctic winter model atmospheres.

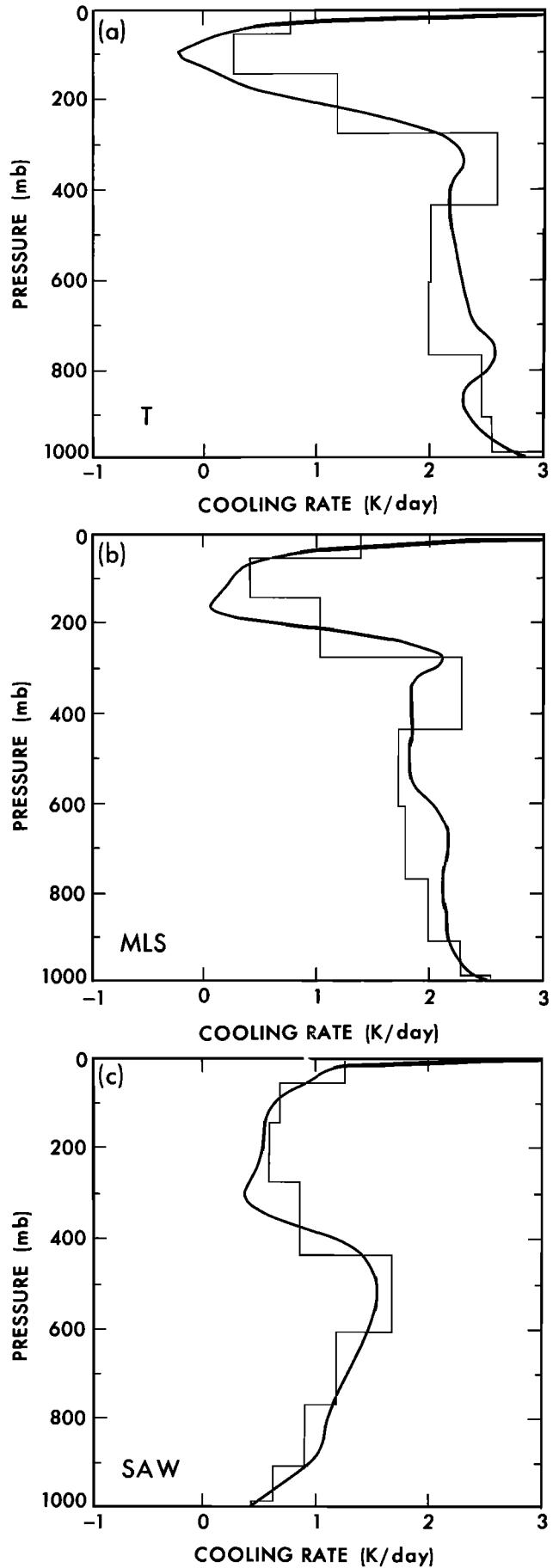


Fig. 2. Cooling rate profiles ($K d^{-1}$) from version II of the GFDL Manabe-Stone model for (a) tropical, (b) mid-latitude summer, and (c) subarctic winter model atmospheres.

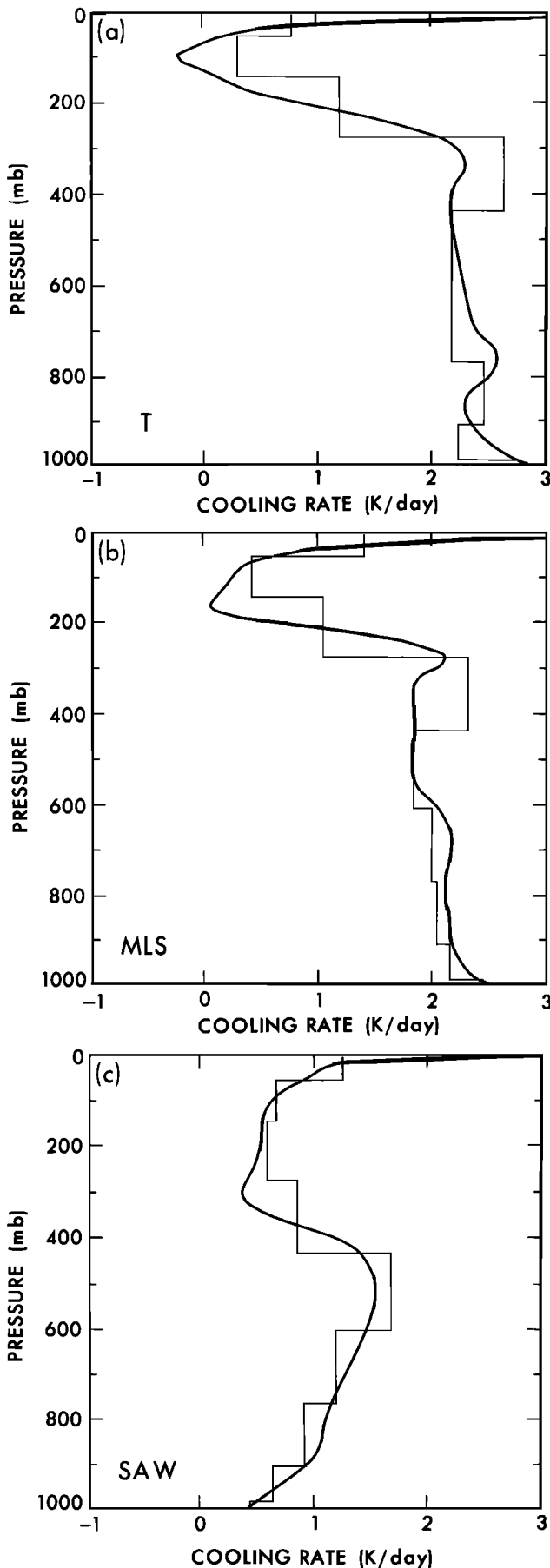


Fig. 3. Cooling rate profiles (K d^{-1}) from version III of the GFDL Manabe-Stone model for (a) tropical, (b) mid-latitude summer, and (c) subarctic winter model atmospheres.

of overly broad spectral bands in Rodgers and Walshaw's water vapor random model.

Introduction of the Bignell continuum in version II leads to a substantial reduction in the undercooling of the lower troposphere longwave cooling rates. Correction of the code errors in the Bignell continuum formulation (version III) appears to almost entirely eliminate the undercooling. The only remaining error of importance is that near 350 mbar.

Flux Results

Table 2 presents fluxes at the surface, tropopause, and top of the atmosphere for each of the three versions of the Manabe-Stone model for the three standard soundings, along with the LBL results. In addition, the sensitivity of the various fluxes to a doubling of CO_2 is given.

TABLE 2. Comparison of LBL Fluxes With Manabe-Stone GFDL Models

	$F^{\text{net}}(1X)$			$F^{\text{net}}(1X) - F^{\text{net}}(2X)$			
	LBL	Model		LBL	Model		
		I	II		I	II	III
<i>Top</i>							
T	298.3	300.9	298.3	296.2	3.3	3.8	3.6
MLS	289.0	289.0	288.4	286.7	3.0	3.5	3.3
SAW	203.0	201.0	201.1	200.9	1.7	2.1	2.1
<i>Tropopause</i>							
T	288.1	294.8	292.5	290.5	5.8	5.7	5.5
MLS	272.8	271.7	271.4	269.7	5.6	5.6	5.5
SAW	178.2	176.5	176.6	176.4	3.6	3.8	3.8
<i>Surface</i>							
T	66.5	102.4	70.0	64.0	1.3	2.0	0.5
MLS	79.1	103.5	84.3	76.9	1.8	2.2	1.0
SAW	82.9	81.8	82.1	79.1	2.9	2.7	2.6

The tropopause is at 93.7 mbar for the T case; 179 mbar for the MLS case; 282.9 mbar for the SAW case.

At the top of the atmosphere and at the tropopause, the three parameterized models obtain fluxes for the 300 ppmv CO_2 cases with typical errors of a few W m^{-2} ; in view of the other uncertainties associated with climate models, this must be considered quite adequate. In addition, the changes in the fluxes produced by a doubling of CO_2 are generally accurate to within 20%. It is significant that the parameterized models (especially version III) underestimate the meridional gradient in the forcing due to doubled CO_2 by up to 30%. A possible explanation is the neglect of the $10\text{-}\mu\text{m}$ bands of CO_2 . Line-by-line results indicate that $\sim 0.3 \text{ W m}^{-2}$ of the sensitivity to doubled carbon dioxide for the T and MLS cases at the tropopause is due to these bands. At high latitudes, these lines are unimportant, due to the strong temperature dependence of this complex.

The situation at the surface is quite different and rather puzzling. As discussed above, the earliest version of the model has very large lower tropospheric cooling rate errors in the tropics and mid-latitudes; these are reflected in the significant surface flux errors, which are on the order of 30 W m^{-2} . This underestimate of the downward flux at the surface presumably results in a compensating underestimate of the upward sensible and latent heat fluxes from the surface into the atmosphere. In the two later versions of the model, this problem is largely eliminated, since the e -type continuum is now included.

Remarkably enough, however, the surface flux sensitivities to doubled CO₂ show a very different picture. Here, it is the original *p*-type model which most nearly reproduces the LBL results, while the newest model does a very poor job. Closer investigation reveals that the main source of error lies in the omission of the 10- μm complex from any of the parameterized models. LBL calculations indicate that $\sim 0.7 \text{ W m}^{-2}$ of the CO₂ flux sensitivity is due to these lines in the tropical case, and $\sim 0.6 \text{ W m}^{-2}$ in the MLS case. Thus, the apparently good results using version I are fortuitous, and due to an overestimate of the surface flux change due to the 15- μm band complex. Although it is certainly true that changes in the surface flux may not be of the greatest importance for many climate model applications [Kiehl and Ramanathan, 1982], complicated results such as these may be of importance for the interpretation of changes in the surface energy budget.

4. GFDL MODEL RESULTS (FELS-SCHWARZKOPF VERSIONS I AND II)

Model Description and Usage

The Fels-Schwarzopf radiation code has been employed operationally at GFDL in the troposphere-stratosphere-mesosphere GCM ("SKYHI") and in a numerical weather prediction model used by Miyakoda and collaborators. The radiation algorithm is designed to be usable from the surface to about 75 km. Water vapor is treated by means of the simplified exchange approximation of Fels and Schwarzopf [1975], carbon dioxide by precomputation of transmission functions as described in Fels and Schwarzopf [1981], and ozone by the one-band random Malkmus model of Rodgers [1968]. The latter is crudely corrected for Doppler effects using the fast approximate method given by Fels [1979]. In the original (1975) formulation of the algorithm (version I), a *p*-type water vapor continuum with a frequency-dependent absorption coefficient is included in the 800 to 1200 cm^{-1} frequency range. In other implementations of the algorithm, an *e*-type water continuum is included in the region from 560 to 1200 cm^{-1} , with the absorption coefficients being obtained from Roberts *et al.* [1976]. In this version, water vapor spectral data is derived from the 1982 AGFL compilation [Rothman *et al.*, 1983]. The frequency range extends from 0 to 2200 cm^{-1} .

Version I of the Fels-Schwarzopf radiation code has been implemented in the "SKYHI" GCM at GFDL. This model has 40 levels extending from the surface to about 80 km. In view of the large number of levels, we refer the reader to Fels *et al.* [1980] for a description of the vertical structure. In the interest of maintaining a uniform radiation algorithm over a very long integration, this implementation was never changed in the "SKYHI" results described below. The "SKYHI" GCM has been used in a large number of simulation and sensitivity studies, including Fels *et al.* [1980] (effect of altered CO₂ and O₃ levels on the middle atmosphere), Mahlman and Umscheid [1984, 1987] (simulated sudden warming, ultra-high resolution dynamics), Hayashi *et al.* [1984] (simulation of tropical waves), Miyahara *et al.* [1986] (effect of resolved gravity waves on planetary waves), and Hamilton and Mahlman [1988] (dynamics of simulated semiannual oscillation).

The second implementation (version II) of the Fels-Schwarzopf algorithm is used in the numerical prediction models employed at GFDL and at several operational

meteorological centers. This version was used in the model employed to produce the GFDL First Garp Global Experiment (FGGE) level 2b data set [Miyahara *et al.*, 1986]. An 18-level version is currently used in the operational medium range forecast (MRF) model at the National Meteorological Center (NMC), and by the Australian Bureau of Meteorology Research Centre.

Cooling Rate Results

We begin with the results from version I, used in the "SKYHI" model. In view of the large altitude range covered, we shall present figures both in *p* as the vertical coordinate and in $\log p$; the former emphasizes the troposphere and the latter the middle atmosphere.

Figures 4a and 4d show results for the tropical case. We see first of all that the algorithm does very well in the lower troposphere (below ~ 850 mbar), with errors less than 0.1 K d^{-1} . This is quite remarkable in view of the fact that this model does not have an *e*-type continuum. One reason for this agreement is that the frequency-dependent *p*-type continuum coefficients used in this model were crudely based on the actual atmospheric observations of Vigroux [1959] and Saiedy [1960] as summarized by Goody [1964]. In the 500–800 mbar range, the model is seen to undercool by $\sim 0.3 \text{ K d}^{-1}$. A detailed investigation of the errors of the parameterized GFDL model in various frequency ranges is reported by Schwarzopf and Fels [this issue]. From those results it appears that the undercooling results from a number of factors, principally the neglect of continuum absorption from 400 to 800 cm^{-1} (especially in the 500–600 mbar range), and the use of wide spectral intervals in the precomputation of emissivities.

Above 500 mbar, the algorithm gives results quite similar to those of the various versions of the Manabe-Stone algorithm discussed by section 3. This is no accident, since, as described by Fels and Schwarzopf [1975], the present method was designed to be a fast and accurate approximation to Rodgers and Walshaw [1966]. In particular, the 0.2 K d^{-1} overcooling at ~ 300 mbar is due to the use of overly broad frequency intervals in the water vapor random model. This excessive cooling is expected to produce an upper tropospheric cold bias in the model; on the basis of unpublished experiments performed by Schwarzopf and Fels, this might account for about 2 K of the observed 8 K bias.

In the tropical stratosphere, the version I algorithm generally gives very good results, although undercooling is observed in the lower stratosphere, due to problems in the treatment of the 9.6- μm O₃ bands. This seemingly small error (about 0.1–0.2 K d^{-1}) may lead to errors of the equilibrated temperature near 50 mbar of as much as 5–10 K, owing to the large radiative relaxation times in this region. More important, it makes attempts to use this particular model to diagnose vertical motion in this region rather suspect. The large error at the stratopause, which leads to an underestimate in the equilibrated temperature of ~ 5 K, is due to the neglect of several minor bands of CO₂ and O₃, as well as to poor treatment of Voigt effects. Errors in the treatment of the stratosphere are discussed in more detail in the article by Schwarzopf and Fels [this issue].

The MLS results (Figures 4b and 4e) are almost identical to those of the tropical case just described. In the lower and middle stratosphere, exchange of photons with the

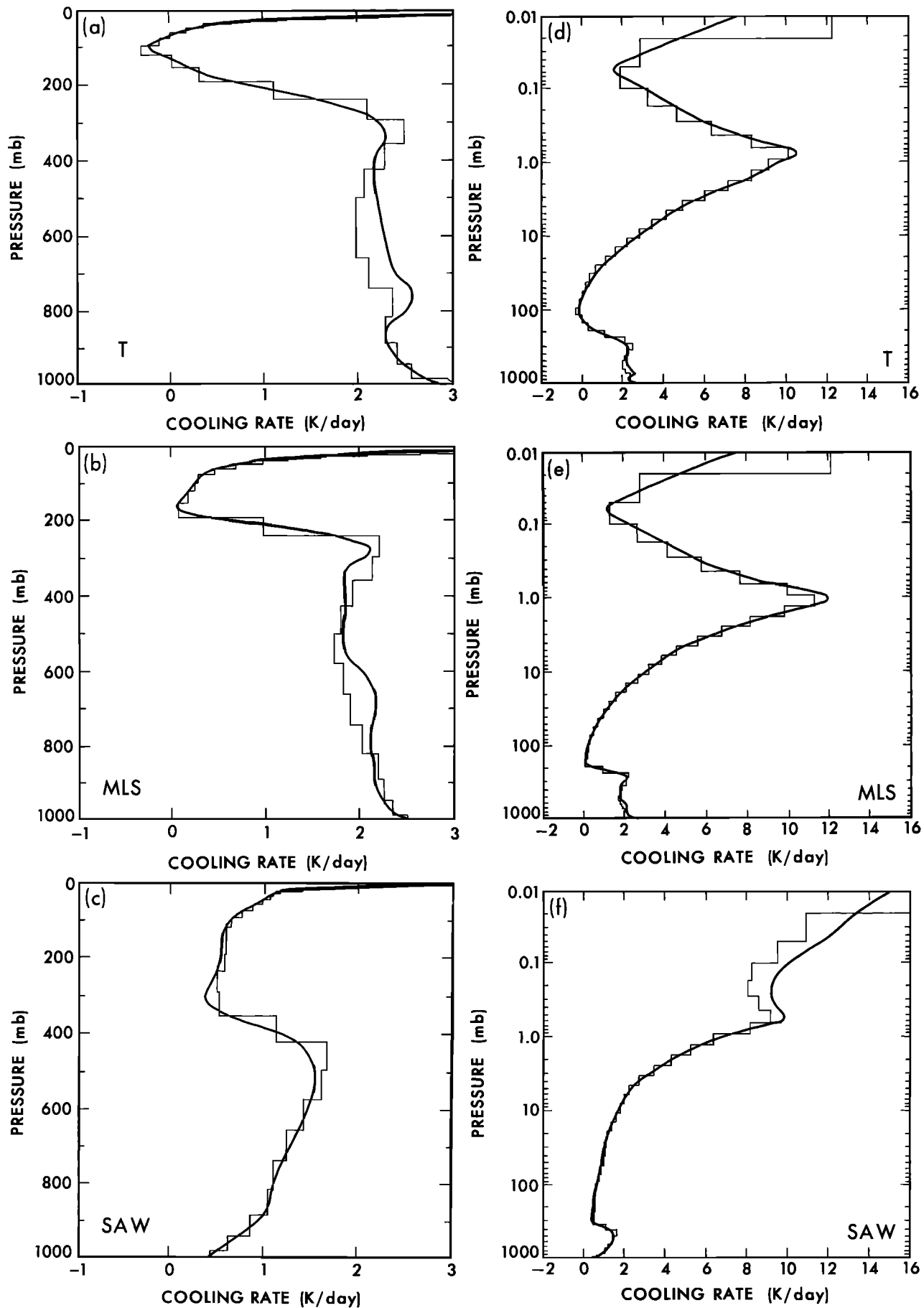


Fig. 4. Cooling rate profiles (K d^{-1}) from version I of the GFDL Fels-Schwarzkopf model for (a) the tropical, (b) the mid-latitude summer, (c) the subarctic winter model profiles, in pressure coordinates. Figures 4d-4f are the same as 4a-4c, but in log pressure coordinates.

lower layers is not as important as in the tropical case, and the errors are thus negligible.

In the subarctic winter calculations shown in Figures 4c and 4f, the atmosphere holds so little water that the continuum plays a minor role; in addition, the effect of the ozone band in heating the lower stratosphere is small. The results therefore show gratifying agreement of operational and benchmark calculations up to ~1 mbar. The comparatively large errors in the mesosphere are largely due to the poor treatment of water vapor in that region (especially the neglect of Doppler effects). In the previous two cases, the cold mesospheric temperatures made this issue less important, but in the polar night, the relative warmth of this region emphasizes any errors made in modeling water vapor opacity.

To illustrate the performance of the Fels-Schwarzkopf model containing an *e*-type water continuum (version II), we shall briefly present results from an implementation for a model with 18 vertical levels. This model employs a σ -coordinate system, with temperatures, cooling rates and mixing ratios carried at sigma levels of 0.021, 0.074, 0.124, 0.175, 0.225, 0.275, 0.325, 0.375, 0.425, 0.497, 0.594, 0.688, 0.777, 0.856, 0.920, 0.981, and 0.995. Figures 5a-5c show the cooling rates calculated for the T, MLS, and SAW soundings, respectively. Above 800 mbar, these results are remarkably similar to the version I Fels-Schwarzkopf parameterization; the sources of the errors (such as the undercooling in the tropical and mid-latitude middle troposphere, and the overcooling at ~325 mbar) have been discussed above. Below 800 mbar, the *e*-type continuum version gives larger errors in the tropical case than does the *p*-type version; it is unclear as to why this is so.

Flux Results

Table 3 presents flux results for these two versions of the Fels-Schwarzkopf model. At the top of the atmosphere, both versions underestimate the outgoing flux by from 3 to 5 W m⁻². In the case of the version II results, some of this error is due to the lack of vertical resolution in the stratosphere. The finite differencing of the transfer equation used in this model assumes that the atmosphere is isothermal above the highest level at which temperature is specified—about 20 mbar for this model. Comparisons with a 40-layer implementation of version II show that

TABLE 3. Comparison of LBL Fluxes With Fels-Schwarzkopf GFDL Models

	$F^{net}(1X)$			$F^{net}(1X) - F^{net}(2X)$		
	Model		Model	Model		Model
	LBL	I		II	LBL	
<i>Top</i>						
T	298.3	293.9	293.6	3.3	3.0	3.2
MLS	289.0	284.4	284.4	3.0	2.7	3.1
SAW	203.0	200.6	200.2	1.7	1.8	2.1
<i>Tropopause</i>						
T	288.1	284.1	286.8	5.8	5.7	5.2
MLS	272.8	268.6	270.6	5.6	5.5	5.2
SAW	178.2	177.7	175.8	3.6	3.8	3.7
<i>Surface</i>						
T	66.5	70.6	62.4	1.3	1.9	0.2
MLS	79.1	77.2	79.1	1.8	2.2	0.4
SAW	82.9	76.3	82.1	2.9	2.9	2.6

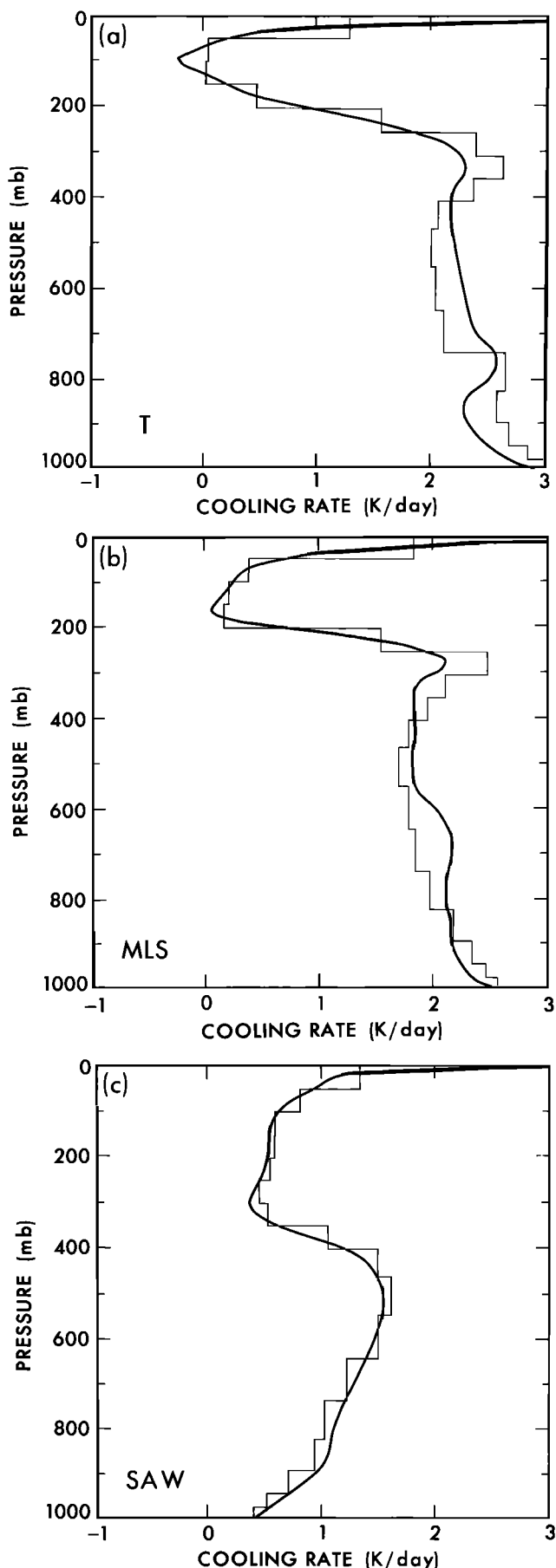


Fig. 5. Cooling rate profiles (K d⁻¹) from version II of the GFDL Fels-Schwarzkopf model for (a) tropical, (b) mid-latitude summer, and (c) subarctic winter profiles.

about 2 W m^{-2} of the error can be accounted for by this mechanism. At the tropopause, the calculations using version I similarly make errors in the net flux of $3\text{--}5 \text{ W m}^{-2}$, while the version II implementation results in a smaller error. At the surface, the version II calculations also appear to result in smaller errors, except for the tropical calculations.

Differences in the forcing due to doubled CO_2 at the top of the atmosphere, tropopause, and surface are remarkably similar to those obtained for the Manabe-Stone simulations, with the present version I calculations being similar to the Manabe-Stone version I results, and the present version II calculations paralleling the version III Manabe-Stone results. Thus, the large difference between the Fels-Schwarzkopf version I and II surface flux sensitivities reflects the omission of the $10\text{-}\mu\text{m}$ band of CO_2 in the parameterized calculations; calculations using the e -type continuum actually give more realistic sensitivities than those of version I.

5. NCAR COMMUNITY CLIMATE MODEL VERSION 0 (CCM0) RESULTS

Over the past 7 years, two versions (0 and 1) of the NCAR CCM have been made available to the atmospheric science community. The CCM is a spectral model that has been run at a number of horizontal resolutions. The model employs a σ -vertical coordinate system. CCM0 was made available to the community in 1983 and has been used for a large number of climate and forecast studies. It has been employed in CO_2 climate studies [Washington and Meehl, 1983, 1984]. A study of the impact of radiative processes on the climate simulation produced by the model was carried out by Ramanathan *et al.* [1983]. Numerous paleoclimate studies also have been performed with the model [Barron and Washington, 1982, 1984; Kutzbach and Guetter, 1986]. The response of the model to imposed sea-surface temperature anomalies was studied by Blackmon *et al.* [1983, 1986]. Forecast studies include the work of Errico [1984], Baumhefner [1983], and Rasch [1985a,b].

CCM0 Model Description

The nine sigma levels in CCM0 are located at 0.991, 0.926, 0.811, 0.664, 0.500, 0.336, 0.189, 0.074, and 0.009. The longwave radiation scheme employed in CCM0 is described by Ramanathan *et al.* [1983]. The method for calculating longwave fluxes and heating rates is based on the absorptivity-emissivity formulation. The absorption due to water vapor, carbon dioxide, and ozone is represented by analytical functions of the absorption for the entire band structure. The frequency range is assumed to extend from 0 to 2200 cm^{-1} .

The longwave fluxes due to water vapor are based on the scheme of Sasamori [1968]. However, the treatment of the emissivity for this scheme was modified by Ramanathan *et al.* [1983] to differentiate between the absorptivity and emissivity. Essentially, the emissivity was determined by dividing the absorptivity by a factor dependent on the pressure-scaled water vapor amount. The functional form of this factor was obtained by fitting data from the Rodgers and Walshaw [1966] band model. Sasamori's scheme does not explicitly account for the absorption by the e -type continuum. However, it is not clear from the description of the model whether continuum absorption has been accounted for or not. It has been recognized for some time that this continuum plays a significant radiative role in

the lower troposphere. As we shall see, this leads to large differences between the lower tropospheric cooling rates in CCM0 as compared to CCM1.

The radiative treatment of carbon dioxide is based on the broadband model of Ramanathan [1976]. The CCM0 broadband model explicitly assumes that all bands in the $15\text{-}\mu\text{m}$ band system overlap one another and that these bands are in the square root limit. The method also explicitly accounts for the temperature dependence of the "hot" bands. Overlap between CO_2 and H_2O rotational lines is accounted for by multiplying the CO_2 band absorptance by the H_2O transmissivity obtained from the Rodgers and Walshaw model. No overlap between the e -type continuum and the CO_2 absorption is included. Ozone is included by employing the band absorptance model of Rodgers [1968].

Cooling Rate Results

The cooling rates from CCM0 are compared with LBL cooling rates for the T, MLS, and SAW profiles in Figures 6a-6c. Once again, these results are dependent on the level structure employed, but it is apparent that the model severely underpredicts the cooling in the lower tropical troposphere by as much as 1 K d^{-1} , which may be related to the manner in which the continuum is included or excluded in the Sasamori water vapor scheme. For the SAW profile, CCM0 actually cools slightly more in the lower troposphere than the LBL results.

Flux Results

Flux results for CCM0 appear in Table 4. The results for the net flux at the tropopause suggest significant differences between the LBL results and the CCM0 model. However, as will be shown later, the fluxes at this level are very sensitive to the model level structure. This conclusion is also supported by the good agreement between the CCM0 model and the LBL results for the top of the atmosphere (within 1.5 W m^{-2}).

The results for the surface-troposphere forcing due to doubled CO_2 indicate that CCM0 is in good agreement with the LBL results (with errors of less than 14%). This agreement, however, must be viewed with some caution, since the actual location of the tropopause in the nine-level model CCM0 is difficult to determine. Kiehl and Briegleb [this issue] compare results from CCM0 employing the ICRCM MLS profile and find larger differences between CCM0 and the LBL results than appear in Table 4. At the surface, the neglect of the water vapor overlap with the $15\text{-}\mu\text{m}$ CO_2 band [Kiehl and Ramanathan, 1982] results in a substantial overestimation of the flux change for the tropical and mid-latitude profiles. For the subarctic winter profile, agreement between CCM0 and the LBL results is quite good, since water vapor overlap is not important for this particular sounding.

6. NCAR COMMUNITY CLIMATE MODEL VERSION 1 (CCM1) RESULTS

CCM1 Model Description

CCM1 was released for community use in 1987. The model has been used in a stratospheric version for a number of studies [Boville, 1986; Boville and Randel, 1986; Kiehl and Boville, 1988; Kiehl *et al.*, 1988]. One of the most significant differences between CCM0 and CCM1 is actually related to changes in the longwave radiation scheme employed in these two versions of the CCM.

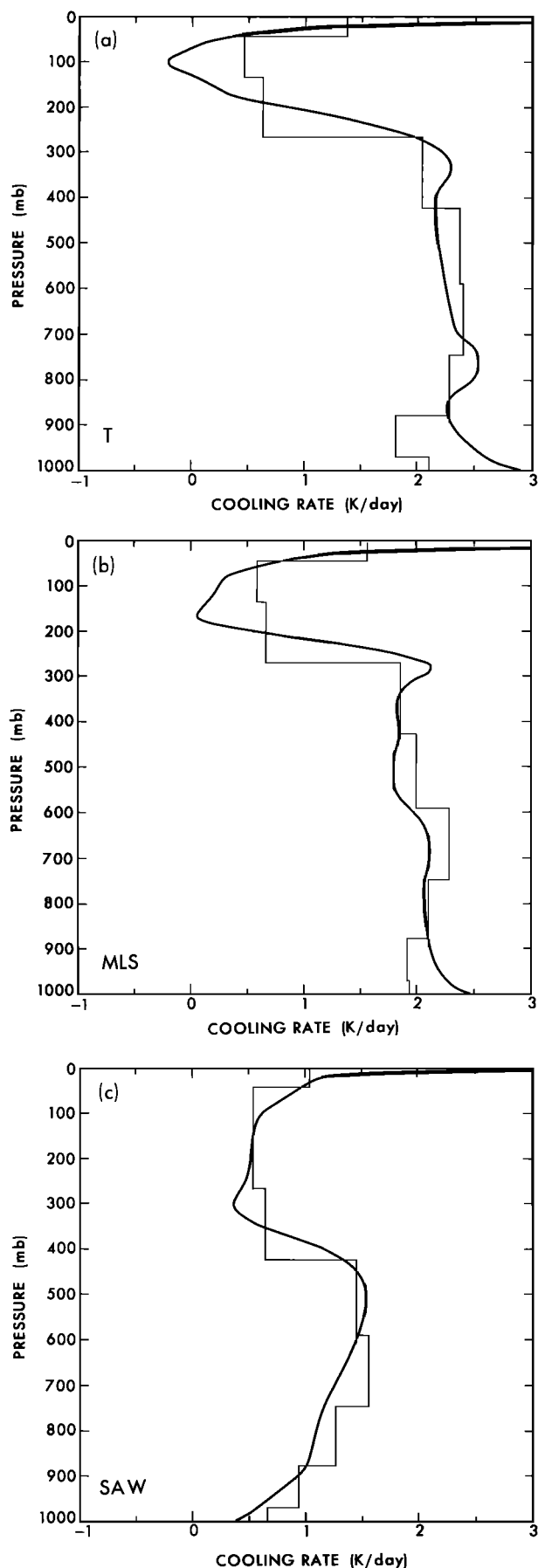


Fig. 6. Cooling rate profiles (K d^{-1}) from the NCAR CCM0 for (a) tropical, (b) mid-latitude summer, and (c) subarctic winter profiles.

TABLE 4. Comparison of LBL Fluxes With CCM0 Model

	$F^{\text{net}}(1X)$		$F^{\text{net}}(1X) - F^{\text{net}}(2X)$	
	LBL	CCM0	LBL	CCM0
<i>Top</i>				
T	298.3	297.3	3.3	4.8
MLS	289.0	285.3	3.0	4.5
SAW	203.0	199.8	1.7	2.8
<i>Tropopause</i>				
T	288.1	292.5	5.8	5.1
MLS	272.8	268.7	5.6	5.0
SAW	178.2	185.9	3.6	3.2
<i>Surface</i>				
T	66.5	87.2	1.3	2.6
MLS	79.1	88.1	1.8	2.8
SAW	82.9	82.7	2.9	2.7

Therefore, it is of great interest to compare both versions of the model to the LBL results. CCM1 has 12 sigma levels, where two additional levels near the tropopause region and one level near the top of the model were added. The 12 sigma levels are located at 0.991, 0.926, 0.811, 0.664, 0.500, 0.355, 0.245, 0.165, 0.110, 0.060, 0.025, and 0.009. Details of the radiation scheme employed in CCM1 can be found in *Kiehl et al.* [1987]. The frequency range extends from 0 to 3000 cm^{-1} , with absorptivities computed to 2200 cm^{-1} .

The water vapor scheme of Sasamori has been replaced by the nonisothermal absorptivity/emissivity model of *Ramanathan and Downey* [1986]. This scheme does include absorption by both the *e*- and *p*-type continua. The *e*-type continuum is based on *Roberts et al.* [1976], while the *p*-type is taken from *Kneizys et al.* [1980] (for details see *Ramanathan and Downey* [1986]). It also accounts for the temperature dependence of the path lengths and the emitting temperature of the source region. Also, the form of the emissivity and absorptivity functions asymptotes for small water vapor amounts to the correct absorption limits, unlike the Sasamori scheme. The broadband carbon dioxide scheme of *Ramanathan et al.* [1983] has been replaced by the scheme of *Kiehl and Briegleb* [this issue]. The major difference between these two models is that the *Kiehl and Briegleb* [this issue] model no longer assumes that all CO_2 bands in the $15\text{-}\mu\text{m}$ region are completely overlapped and in the square root limit. The weaker "hot" bands have been separated from the band center and their functional form is sufficiently general to account for the linear and logarithmic asymptotic limits of absorption. The ozone absorption parameterization of Rodgers has been replaced by the broadband model of *Ramanathan and Dickinson* [1979]. Finally, the numerical algorithm for evaluating the integral exchange term has been improved in CCM1; nearest layers are subdivided to increase the accuracy of evaluating the absorption functions over that layer.

Cooling Rate Results

Cooling rates for the CCM1 model are compared with the LBL results for the T, MLS, and SAW profiles in Figures 7a-7c. The cooling in the tropical and mid-latitude summer lower troposphere has been considerably enhanced over that due to the CCM0 model. If anything, CCM1 cools somewhat more ($0.3\text{--}0.4 \text{ K d}^{-1}$) than the LBL results. Cooling rates for the SAW profile indicate very good agreement between CCM1 and the LBL model.

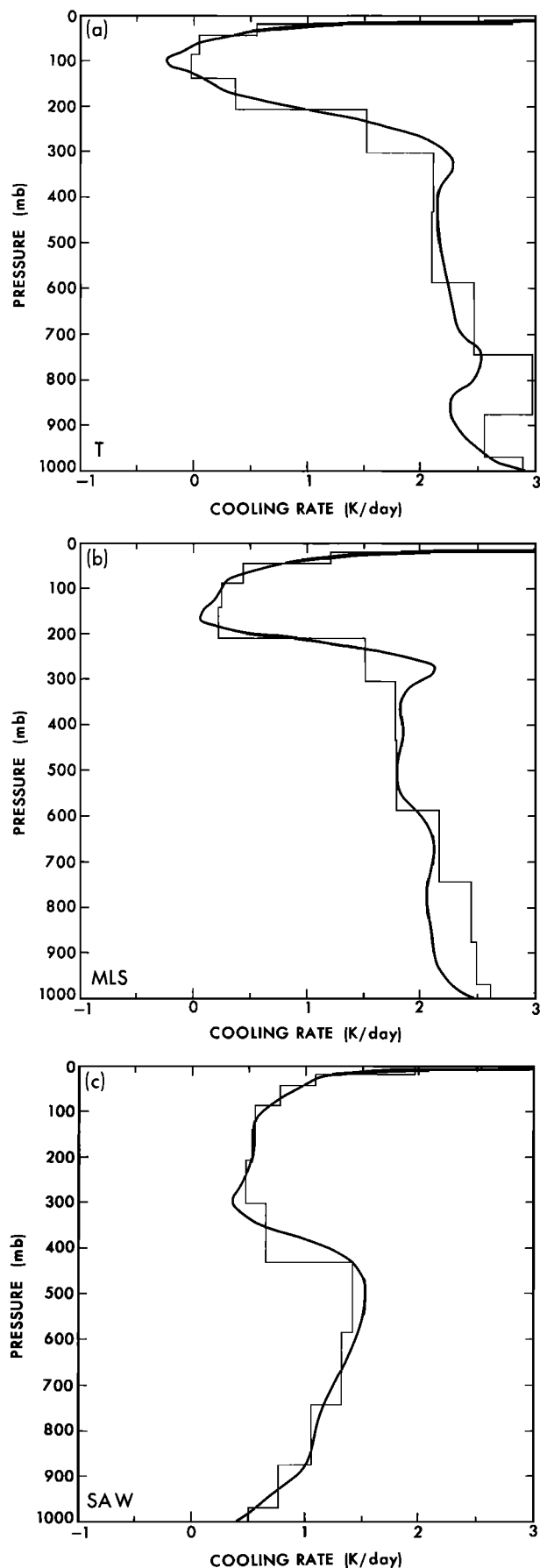


Fig. 7. Cooling rate profiles (K d^{-1}) from the NCAR CCM1 for (a) tropical, (b) mid-latitude summer, and (c) subarctic winter profiles.

Flux Results

Flux results for CCM1 are presented in Table 5. Net fluxes at the tropopause from the CCM1 agree with the LBL values to within approximately 3% in the tropics. As we will see, most of this discrepancy is due to level structure differences; agreement at the top is somewhat better, to within $\sim 3 \text{ W m}^{-2}$. In particular, the greatest discrepancy, 4.6 W m^{-2} , occurs in the tropics where the tropopause structure is sharper than at other latitudes. For the MLS case, the CO_2 tropopause forcing obtained from CCM1 is lower than that calculated from the LBL model. However, as noted by section 3, $\sim 0.6 \text{ W m}^{-2}$ of the CO_2 forcing arises from bands other than the $15\text{-}\mu\text{m}$ band system; Kratz *et al.* [this issue], using a narrow-band model, obtain a similar value ($\sim 0.45 \text{ W m}^{-2}$). Therefore the LBL $15\text{-}\mu\text{m}$ forcing for the MLS is closer to 5.0 W m^{-2} . Kiehl and Briegleb [this issue] show for the CO_2 -only case that the CCM1 broadband model forcing due to a doubling differs from the LBL results by 0.45 W m^{-2} . Thus, $\sim 0.2 \text{ W m}^{-2}$ difference in the forcing remains unexplained and could be due to the overlap treatment between H_2O and CO_2 . The CO_2 forcing results at the surface for the tropical and mid-latitude profiles have decreased dramatically due to the inclusion of H_2O overlap. These fluxes are still at variance with the LBL results due to the neglect of other CO_2 bands included in the LBL calculations.

TABLE 5. Comparison of LBL Fluxes With CCM1 Model

	$F^{\text{net}}(1X)$		$F^{\text{net}}(1X) - F^{\text{net}}(2X)$	
	LBL	CCM1	LBL	CCM1
<i>Top</i>				
T	301.2	297.4	3.3	4.3
MLS	290.2	286.7	3.0	4.1
SAW	203.4	199.5	1.7	2.6
<i>Tropopause</i>				
T	291.0	295.6	5.8	4.9
MLS	274.0	277.5	5.6	4.8
SAW	178.6	179.2	3.6	3.4
<i>Surface</i>				
T	69.4	68.1	1.3	0.4
MLS	80.3	81.0	1.8	0.6
SAW	83.3	91.2	2.9	2.3

A More Detailed Comparison

In order to better understand the differences shown in Tables 4 and 5 and Figures 6 and 7, we will consider a number of quantities that could affect these results. In particular, we carry out a more detailed comparison of CCM1 and CCM0. We also consider the effects of vertical resolution on the comparison of CCM1 with the LBL results, and furthermore the contribution of individual gases to the total fluxes.

Table 6 summarizes the comparison of the outgoing flux at 9 mbar, the downward flux at the surface, and the mass weighted heating rates and their differences.

These results confirm that there is good agreement between the top-of-atmosphere fluxes, but they also point to large differences in the downward flux at the surface. The largest difference is in the tropics and indicates the importance in the changes in the water vapor scheme between CCM0 and CCM1. The mass-weighted cooling rate differences are insignificant, but there are dramatic

TABLE 6. Comparison of CCM0 and CCM1 Fluxes Using Same Level Structure From McClatchey Profiles

	CCM1	CCM0	Δ
T			
F(top)	303.2	303.8	0.6
F(surf)	391.2	372.0	-19.2
Q	-1.9	-1.8	0.1
MLS			
F(top)	292.9	293.0	0.1
F(surf)	342.6	335.5	-7.1
Q	-1.7	-1.6	0.1
SAW			
F(top)	203.6	205.4	1.8
F(surf)	156.6	165.0	8.5
Q	-0.9	-1.0	-0.1

differences in the vertical heating between the two models. This is illustrated in Figures 8a-8c, where the heating rates for the three atmospheric profiles are shown for CCM0 and CCM1. For the tropical profile, heating differences in the lower troposphere are as large as 1 K d⁻¹. For the MLS profile, differences are still large (greater than 0.5 K d⁻¹) where CCM1 cools more than CCM0. For the SAW profile, CCM1 actually cools less than the CCM0 model. These results indicate the value of considering the surface radiative fluxes for model validation purposes, since the top-of-atmosphere fluxes are less sensitive to the H₂O continuum absorption.

The question remains as to how important differences in the vertical resolution are to the comparison of operational model results and the LBL results. To address this issue, fluxes from the CCM1 model have been evaluated on the same high-resolution vertical grid that was employed for the LBL calculations. Table 7 compares the net fluxes at three levels of the two models for the tropical profile; also included are the mass-weighted atmospheric heating rates from the models.

The agreement between these two models is now much better at the tropopause than was found in Table 5. This indicates that differences in vertical resolution are the main source of differences between CCM1 and LBL absolute fluxes. To further understand the differences in Table 7, the total fluxes have been broken down into contributions from individual gases. Table 8 lists the values of the net flux at the tropopause for the tropical profile for water vapor and carbon dioxide. Further comparisons for CO₂ are presented by Kiehl and Briegleb [this issue]. Differences due to ozone are much smaller than those due to either of these gases.

The results of Table 8 indicate that the major source of the differences arises from the water vapor treatment. This is most likely due to the narrow-band model data employed by Ramanathan and Downey [1986] to obtain their parameterization, which used a random model with a 5 cm⁻¹ interval width. It is now recognized [Schwarzkopf and Fels, this issue] that a random model interval width of 10 cm⁻¹ is more appropriate for water vapor transmission calculations for these types of models. Finally, another source of bias could arise from the overlap treatment of the gases, which is an inherent problem with broadband models.

Summary

These results indicate that a significant improvement in modeling longwave radiative processes in the CCM

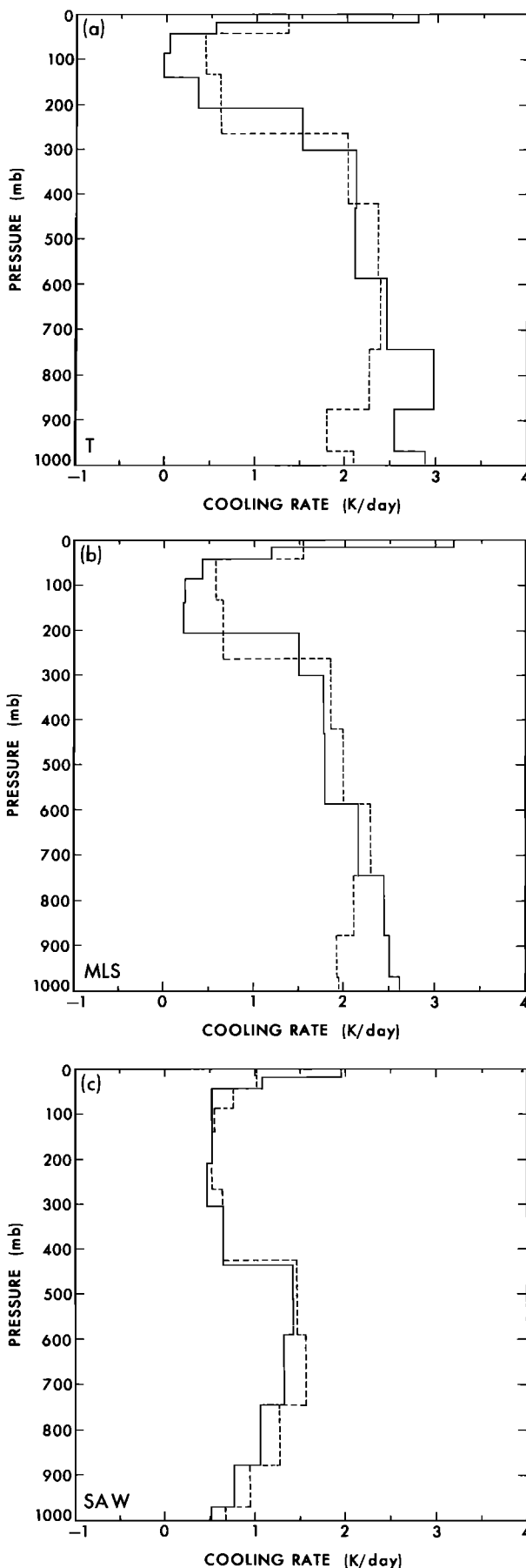


Fig. 8. Cooling rate profiles (K d⁻¹) from CCM0 (dashed line) and CCM1 (solid line) for (a) tropical, (b) mid-latitude summer, and (c) subarctic winter profiles.

TABLE 7. Comparison of LBL and CCM1 Absolute Fluxes Employing Same High Vertical Resolution Grid on a Tropical Sounding

	LBL	CCM1	Δ
$F^{\text{net}}(\text{top})$	301.2	302.2	1.0
$F^{\text{net}}(\text{trop})$	291.0	293.2	2.2
$F^{\text{net}}(\text{surf})$	69.4	71.9	2.5
Q	-1.9	-1.9	0.0

TABLE 8. Flux Contributions From CO₂ and H₂O for LBL and CCM1

	LBL	CCM1	Δ
H ₂ O	334.4	336.3	1.9
CO ₂	405.1	404.3	-0.8

has occurred in going from version 0 to version 1. The majority of this improvement was achieved by employing the Ramanathan and Downey water vapor scheme. Changes in the level structure and in the vertical finite difference scheme have also aided in the accuracy of the cooling rate calculations.

7. GODDARD INSTITUTE FOR SPACE STUDIES MODEL RESULTS (MODEL II [Hansen et al., 1983])

Model Description and Usage

The Goddard Institute for Space Studies (GISS) GCM radiation model has been used for climate modeling in basically unaltered form since 1983. It is described briefly by Hansen et al. [1988], and has been used primarily for tropospheric modeling with nine sigma layers between ground and 10 mbar.

A detailed description of the radiation scheme is given by Lacis and Oinas [this issue]. Integration over the thermal spectrum utilizes the correlated k -distribution method to treat gaseous absorption and emission in a vertically inhomogeneous atmosphere. The model uses 11 composite k -distribution intervals for H₂O, 10 for CO₂, and four for O₃ to cover the thermal spectrum. Absorption coefficients in these composite intervals are determined by merging Planck function weighted narrow band k -distributions ($\sim 50 \text{ cm}^{-1}$) from noncontiguous spectral regions. The narrow band k -distributions are obtained from Malkmus model parameters that are least squares fitted to LBL transmissions calculated using the AFGL line compilation [Rothman, 1981] for a grid of pressure and temperature combinations. Absorption contributions due to CH₄, N₂O, CFCl₃, and CF₂Cl₂ and the weaker bands of H₂O, CO₂, and O₃ are included as absorption overlapping. Water vapor continuum absorption is included using the formulation and spectral dependence given by Roberts et al. [1976]. Absorption coefficients representing the merged k -distribution intervals are interpolated as functions of pressure, temperature, and absorber amount from a large table of Planck function weighted coefficients. The atmospheric temperature profile is specified at layer edge points and is assumed to be linear in Planck function within the layer interior. This permits the integrated thermal emission from the entire layer to be obtained in closed form. The frequency range extends from 0 to 2500 cm^{-1} .

The sensitivity of the GISS GCM to climate forcing and feedback analysis is presented by Hansen et al. [1984] for doubled CO₂, for a 2% solar constant increase, and for Ice Age simulations. Model simulations of transient climate change due to the anthropogenic increase of CO₂ and other trace gases, along with projections into the future, are compared with the observed global temperature record by Hansen et al. [1988]. Other studies describing climate simulations with the GISS GCM include analysis of doubled CO₂ experiment results by Rind [1987a, 1988] and of paleoclimate simulations by Rind and Petet [1985] and Rind [1986, 1987b]. Application of the GISS GCM radiation model for stratospheric modeling is described by Rind et al. [1988].

The radiative algorithm described above has been applied to two different vertical layer structures, set according to the sigma-level prescription used in the tropospheric and stratospheric versions of the GISS GCM. The results computed with the tropospheric 12-layer version are designated as "model A" results, while those for the stratospheric 25-layer version are designated as "model B" results. It should be emphasized that cooling rates from models A and B are calculated using the same radiative model and the same set of k -distribution absorption coefficient tables.

Cooling Rate Results

Cooling rates computed with model A are shown in Figures 9a-9c for the T, MLS, and SAW temperature profiles. The GCM results are generally in good agreement with the LBL results, particularly for the SAW profile, where agreement is very close throughout the atmosphere. In the case of the T and MLS profiles, the upper tropospheric and stratospheric cooling rates closely follow the LBL results, but there is a marked overestimate of the cooling below the 800-mbar pressure level. Surprisingly, the error appears largely to result from the computation of cooling rates due to absorption lines, not in the formulation of the water vapor continuum. Figure 10 shows that the $\sim 0.5 \text{ K d}^{-1}$ cooling rate error persists in the lower two model layers even for the noncontinuum case for the MLS profile. The reasons for this error (and the good agreement for the SAW profile) are unclear.

Figures 11a-11c show a comparison of cooling rates using model B for the T, MLS, and SAW profiles. All three profiles show good agreement with the LBL results below ~ 1 mbar, although the GCM results for the T and MLS profiles still overestimate the near-surface cooling as in the case of the tropospheric model. The T and MLS cooling is in general agreement with the LBL results up to the 0.1-mbar level, while the SAW profile results overestimate the cooling by 2-3 K d^{-1} . Part of the cooling rate difference with respect to the LBL cooling above the 1-mbar level stems from differences in the pressure-temperature interpolation method of the McClatchey temperature profiles between the GCM and LBL calculations. Undoubtedly, as in the case of the GFDL model, errors in modeling the water vapor opacity also contribute to these differences.

Flux Results

Table 9 compares the net fluxes computed for models A and B against LBL results for the three standard temperature profiles. The net fluxes at the top of the atmosphere are found to agree within $\sim 1 \text{ W m}^{-2}$ of the

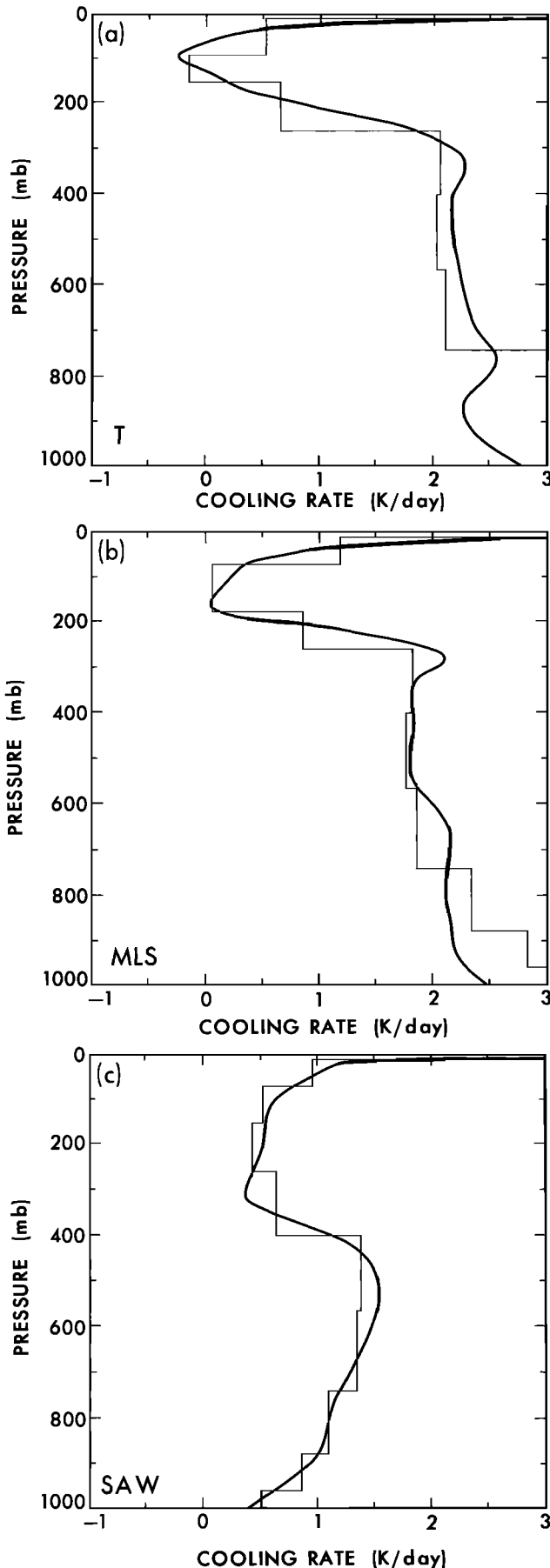


Fig. 9. Cooling rate profiles (K d^{-1}) from the 12-layer GISS model (model A) for (a) tropical, (b) mid-latitude summer, and (c) subarctic winter profiles.

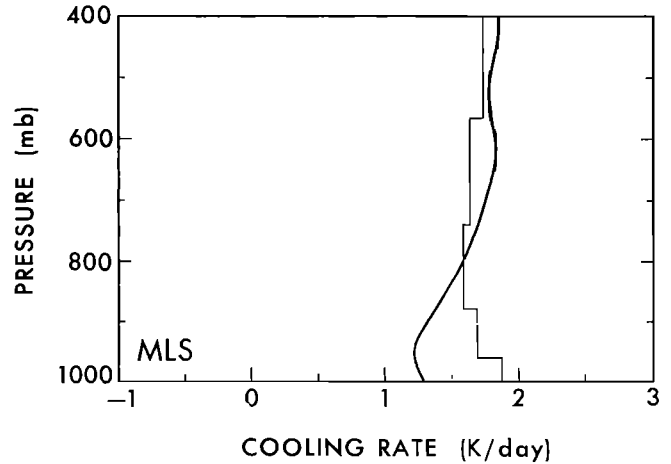


Fig. 10. Cooling rate profiles (K d^{-1}) for the case of no water vapor continuum from LBL (solid line) and GISS model (vertical line) for the mid-latitude summer profile.

LBL results for both models A and B for the T, MLS, and SAW profiles. At the tropopause, the agreement is within $\sim 2 \text{ W m}^{-2}$. To avoid interpolation errors, the layer edges were shifted to coincide with the 17, 13 and 9 km levels (93.7, 179.0, and 282.9 mbar) for the T, MLS, and SAW profiles, respectively. The differences between models A and B, and between the LBL results at the atmosphere, top, and tropopause, are percentage-wise small and appear to be random.

The largest net flux errors are in the surface net flux results. Here, models A and B give essentially identical results (because of similar tropospheric layering structure), but there does appear to be a systematic trend with an overestimate of the net flux by 3.5 W m^{-2} for the SAW profile and an underestimate by 5.1 W m^{-2} in the case of the T profile. As in the case of the cooling rate comparisons, it is not clear that a simple explanation for the net flux differences is possible.

The sensitivity of the net flux to doubled CO_2 is also compared in Table 9. Here again, the differences between the tropospheric and stratospheric versions of the GCM are minimal, being generally less than 0.1 W m^{-2} . At the top of the atmosphere and the tropopause, the GCM results show a $\sim 0.7 \text{ W m}^{-2}$ larger net flux change than obtained with the LBL calculations. At the surface, the GCM net flux change is within $\sim 0.1 \text{ W m}^{-2}$ of the LBL results for the T and MLS profiles. However, there is a dramatic difference of 1.6 W m^{-2} in the case of the SAW profile for doubled CO_2 . These differences likewise do not have an immediate explanation.

8. SUMMARY

This study has focused on the relative accuracy of radiation parameterizations used in operational general circulation models at three institutions. The general conclusion from this study is that the most recent versions of the radiation parameterizations agree quite well with the benchmark LBL model results. In particular, the cooling rate profiles from these models are in fairly good agreement with the benchmark cooling rates. In some ways this is not surprising, since these parameterizations have been developed with the use of these benchmark results.

Uncertainties with regard to the parameterization of the water vapor continuum are still of major concern.

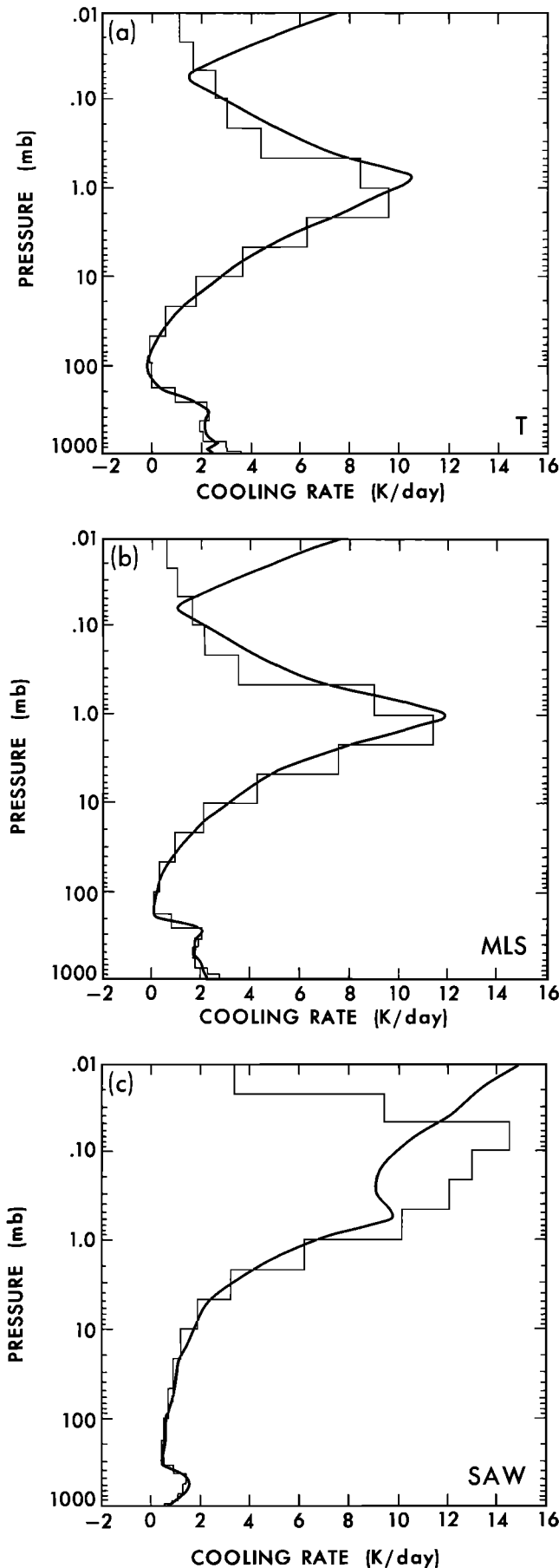


Fig. 11. Cooling rate profiles (K d^{-1}) from the 25-layer GISS model (model B) for (a) tropical, (b) mid-latitude summer, and (c) subarctic winter profiles.

TABLE 9. Comparison of Fluxes From the GISS GCM With Line-by-Line Results

	$F^{\text{net}}(1X)$		$F^{\text{net}}(1X) - F^{\text{net}}(2X)$			
	Model		Model			
	LBL	A	B	LBL	A	B
<i>Top</i>						
T	299.0	297.6	298.4	3.2	4.0	4.1
MLS	289.5	290.2	290.1	3.0	3.7	3.8
SAW	203.1	202.5	202.7	1.7	2.3	2.2
<i>Tropopause</i>						
T	288.7	286.9	288.8	5.8	6.7	6.7
MLS	273.3	274.7	274.7	5.6	6.5	6.4
SAW	178.3	180.4	179.8	3.6	4.3	4.3
<i>Surface</i>						
T	67.1	62.0	62.0	1.3	1.2	1.2
MLS	79.5	77.3	77.4	1.8	1.9	1.9
SAW	83.0	86.5	86.5	2.9	4.5	4.5

The importance of this process to tropical and mid-latitude lower tropospheric cooling is significant and can be important in the simulation of convective activity in the general circulation models. It is important that our knowledge of this process be extended in the next few years. It is also apparent from this study that an attempt should be made to parameterize the weaker absorption bands of CO_2 and O_3 , in order to obtain more accurate agreement with the LBL results.

As with any parameterization process, the development of radiation codes is not static. We hope that as newer versions of operational model radiation codes become available, they are continually compared with benchmark calculations and improved observational data, and that the results of these comparisons be made available to the general circulation modeling community.

Acknowledgments. It is unfortunate that during the preparation of this manuscript, Steve Fels passed away. Steve asked me (J.T.K.) to assume responsibility for the completion of the manuscript a month before his death. Much of the study carries with it the mark of his erudite style; he shall be missed by his friends and colleagues. J.T.K. would like to thank Bruce Briegleb for preparing the NCAR CCM results. The National Center for Atmospheric Research is sponsored by the National Science Foundation.

REFERENCES

- Barron, E. J., and W. M. Washington, The Cretaceous atmospheric circulation: Comparisons of model simulations with the geologic record, *Paleogeogr. Paleoclim. Paleocol.*, **40**, 103–133, 1982.
- Barron, E. J., and W. M. Washington, The role of geographic variables in explaining paleoclimates: Results from Cretaceous climate model sensitivity studies, *J. Geophys. Res.*, **89**, 1267–1279, 1984.
- Baumhefner, D. P., Relationship between present large-scale forecast skill and new estimates of predictability error growth, Proceedings, Workshop on Predictability of Fluid Motions, vol. 106, pp. 169–180, Am. Inst. of Phys., New York, 1983.
- Bignell, K. J., The water-vapour infra-red continuum, *Q. J. R. Meteorol. Soc.*, **96**, 390–403, 1970.
- Blackmon, M. L., J. E. Geisler, and E. J. Pitcher, A general circulation model study of January climate anomaly patterns associated with interannual variation of equatorial Pacific sea surface temperatures, *J. Atmos. Sci.*, **43**, 1410–1425, 1983.
- Blackmon, M. L., S. L. Mullen, and G. T. Bates, The climatology of blocking events in a persistent January simulation with a spectral general circulation model, *J. Atmos. Sci.*, **43**, 1379–1405, 1986.

- Boville, B. A., Wave-mean flow interactions in a general circulation model of the troposphere and stratosphere, *J. Atmos. Sci.*, **43**, 1711–1725, 1986.
- Boville, B. A., and W. J. Randel, Observations and simulation of the variability of the stratosphere and troposphere in January, *J. Atmos. Sci.*, **43**, 3015–3034, 1986.
- Broccoli, A. J., and S. Manabe, The influence of continental ice, atmospheric CO₂, and land albedo on the climate of the last glacial maximum, *Clim. Dyn.*, **1**, 87–99, 1987.
- Bryan, K., F. G. Komro, S. Manabe, and M. J. Spelman, Transient climate response to increasing atmospheric carbon dioxide, *Science*, **215**, 56–58, 1982.
- Bryan, K., S. Manabe, and M. J. Spelman, Interhemispheric asymmetry in the transient response of a coupled ocean-atmosphere model to a CO₂ forcing, *J. Phys. Oceanogr.*, **18**, 851–867, 1988.
- Drayson, S. R., Atmospheric transmission in the CO₂ bands between 12 μ and 18 μ, *Appl. Opt.*, **5**, 385–391, 1973.
- Ellingson, R. G., J. Ellis, and S. Fels, The intercomparison of radiation codes in climate models: Longwave results, *J. Geophys. Res.*, this issue.
- Errico, R., The dynamical balance of a general circulation model, *Mon. Weather Rev.*, **112**, 2439–2454, 1984.
- Fels, S. B., Simple strategies for inclusion of Voigt effects in infrared cooling calculations, *Appl. Opt.*, **18**, 2634–2637, 1979.
- Fels, S. B., Analytic representations of standard atmosphere temperature profiles, *J. Atmos. Sci.*, **43**, 219–221, 1986.
- Fels, S. B., and M. D. Schwarzkopf, The simplified exchange approximation: A new method for radiative transfer calculations, *J. Atmos. Sci.*, **32**, 1475–1488, 1975.
- Fels, S. B., and M. D. Schwarzkopf, An efficient, accurate algorithm for calculating CO₂ 15-μm band cooling rates, *J. Geophys. Res.*, **86**, 1205–1232, 1981.
- Fels, S. B., J. D. Mahlman, M. D. Schwarzkopf, and R. W. Sinclair, Stratospheric sensitivity to perturbations in ozone and carbon dioxide: Radiative and dynamical response, *J. Atmos. Sci.*, **37**, 2265–2297, 1980.
- Goody, R. M., *Atmospheric Radiation*, 436 pp., Oxford University Press, New York, 1964.
- Hamilton, K., and J. D. Mahlman, General circulation model simulation of the semiannual oscillation of the tropical middle atmosphere, *J. Atmos. Sci.*, **45**, 3212–3235, 1988.
- Hansen, J. G., G. Russell, D. Rind, P. Stone, A. Lacis, S. Lebedeff, R. Ruedy, and L. Travis, Efficient three-dimensional global models for climate studies: Models I and II, *Mon. Weather Rev.*, **111**, 609–662, 1983.
- Hansen, J., A. Lacis, D. Rind, G. Russell, P. Stone, I. Fung, R. Ruedy, and J. Lerner, Climate sensitivity: Analysis of feedback mechanisms, in *Climate Processes and Climate Sensitivity*, *Geophys. Monogr.*, **29**, edited by J. E. Hansen and T. Takahashi, pp. 130–163, AGU, Washington, D. C., 1984.
- Hansen, J., I. Fung, A. Lacis, D. Rind, S. Lebedeff, R. Ruedy, and G. Russell, Global climate changes as forecast by Goddard Institute for Space Studies three-dimensional model, *J. Geophys. Res.*, **93**, 9341–9364, 1988.
- Hayashi, Y., D. Golder, and J. D. Mahlman, Stratospheric and mesospheric Kelvin waves simulated by the GFDL “SKYHI” general circulation model, *J. Atmos. Sci.*, **41**, 1971–1984, 1984.
- Kiehl, J. T., and B. A. Boville, The radiative-dynamical response of a stratospheric-tropospheric general circulation model to changes in ozone, *J. Atmos. Sci.*, **45**, 1798–1817, 1988.
- Kiehl, J. T., and B. P. Briegleb, A new parameterization of the absorptance due to the 15-μm band system of carbon dioxide, *J. Geophys. Res.*, this issue.
- Kiehl, J. T., and V. Ramanathan, Radiative heating due to increased CO₂: The role of H₂O continuum absorption in the 12–18 μm region, *J. Atmos. Sci.*, **39**, 2923–2926, 1982.
- Kiehl, J. T., B. A. Boville, and B. P. Briegleb, Response of a general circulation model to a prescribed Antarctic ozone hole, *Nature*, **332**, 501–504, 1988.
- Kiehl, J. T., R. J. Wolski, B. P. Briegleb, and V. Ramanathan, Documentation of radiation and cloud routines in the NCAR Community Climate Model (CCM1), National Center for Atmospheric Research, *NCAR Tech. Note NCAR/TN-288+IA*, 109 pp., Boulder, Colo., 1987. (Available as *NTIS PB88-236112/AS* from Natl. Tech. Inf. Serv., Springfield, Va.)
- Kneizys, F. X. et al., Atmospheric transmittance radiance—computer code LOWTRAN5, Environ. Res. Pap. No. 697, AFGL-TR-80-0067, 233 pp., Air Force Geophys. Lab., Bedford, Mass., 1980.
- Kratz, D. P., B.-C. Gao, and J. T. Kiehl, A study of the radiative effects of the 9.4 and 10.4 micron bands of carbon dioxide, *J. Geophys. Res.*, this issue.
- Kutzbach, J. E., and P. J. Guetter, The influence of changing orbital parameters and surface boundary conditions on climate simulations for the past 18,000 years, *J. Atmos. Sci.*, **43**, 1726–1759, 1986.
- Lacis, A. A., and V. Oinas, A description of the correlated *k*-distribution method for modeling nongray gaseous absorption, thermal emission, and multiple scattering in vertically inhomogeneous atmospheres, *J. Geophys. Res.*, this issue.
- Mahlman, J. D., and L. J. Umscheid, Dynamics of the middle atmosphere: Successes and problems of the GFDL “SKYHI” general circulation model, in *Dynamics of the Middle Atmosphere*, edited by J. R. Holton and T. Matsuno, pp. 501–526, Terra Scientific Publishing, Terrapub, Tokyo, 1984.
- Mahlman, J. D., and L. J. Umscheid, Comprehensive modeling of the middle atmosphere: The influence of resolution, in *Transport Processes in the Middle Atmosphere*, edited by G. Visconti and R. Garcia, pp. 251–266, D. Reidel, Hingham, Mass., 1987.
- Manabe, S., and A. J. Broccoli, A comparison of climate model sensitivity with data from the last glacial maximum, *J. Atmos. Sci.*, **42**, 2643–2651, 1985.
- Manabe, S., and R. J. Stouffer, A CO₂-climate sensitivity study with a mathematical model of the global climate, *Nature*, **282**, 491–493, 1979.
- Manabe, S., and R. J. Stouffer, Sensitivity of a global climate model to an increase in CO₂ content of the atmosphere, *J. Geophys. Res.*, **85**, 5529–5554, 1980.
- Manabe, S., and R. T. Wetherald, The effects of doubling of CO₂ concentration on the climate of a general circulation model, *J. Atmos. Sci.*, **32**, 3–15, 1975.
- Manabe, S., and R. T. Wetherald, Large-scale changes in soil wetness induced by an increase in atmospheric carbon dioxide, *J. Atmos. Sci.*, **44**, 1212–1235, 1987.
- McClatchey, R. A., R. W. Fenn, J. E. A. Selby, F. E. Volz, and J. S. Garing, Optical properties of the atmosphere, Environ. Res. Pap. No. 411, AFCRL-72-0497, 108 pp., Air Force Cambridge Res. Lab., Bedford, Mass., 1972.
- Miyahara, Y., Y. Hayashi, and J. D. Mahlman, Interactions between gravity waves and planetary-scale flow simulated by the GFDL “SKYHI” general circulation model, *J. Atmos. Sci.*, **43**, 1844–1861, 1986.
- Ramanathan, V., Radiative transfer within the earth’s troposphere and stratosphere: A simplified radiative-convective model, *J. Atmos. Sci.*, **33**, 1330–1346, 1976.
- Ramanathan, V., and R. E. Dickinson, The role of stratospheric ozone in the zonal and seasonal radiative energy balance of the earth-troposphere system, *J. Atmos. Sci.*, **36**, 1084–1104, 1979.
- Ramanathan, V., and P. Downey, A nonisothermal emissivity and absorptivity formulation for water vapor, *J. Geophys. Res.*, **91**, 8649–8666, 1986.
- Ramanathan, V., E. J. Pitcher, R. C. Malone, and M. L. Blackmon, The response of a spectral general circulation model to improvements in radiative processes, *J. Atmos. Sci.*, **40**, 605–630, 1983.
- Rasch, P. J., Developments in normal mode initialization, Part I, A simple interpretation for normal mode initialization, *Mon. Weather Rev.*, **113**, 1746–1753, 1985a.
- Rasch, P. J., Developments in normal mode initialization, Part II, A new method and its comparison with currently used schemes, *Mon. Weather Rev.*, **113**, 1753–1770, 1985b.
- Rind, D., The dynamics of warm and cold climates, *J. Atmos. Sci.*, **43**, 3–24, 1986.
- Rind, D., The doubled CO₂ climate: Impact of the sea surface temperature gradient, *J. Atmos. Sci.*, **44**, 3235–3268, 1987a.
- Rind, D., Components of Ice Age circulation, *J. Geophys. Res.*, **92**, 4241–4281, 1987b.
- Rind, D., Dependence of warm and cold climate depiction on climate model resolution, *J. Clim.*, **1**, 965–997, 1988.
- Rind, D., and D. Petet, LGM terrestrial evidence and CLIMAP SSTs: Are they consistent, *Quat. Res.*, **24**, 1–22, 1985.

- Rind, D., R. Suozzo, N. K. Balachandran, A. Lacis, and G. Russell, The GISS global climate—middle atmosphere model, Part I, Model, structure and climatology, *J. Atmos. Sci.*, *45*, 329–370, 1988.
- Roberts, R. E., J. E. Selby, and L. M. Biberman, Infrared continuum absorption by atmospheric water vapor in the 8–12 μm window, *Appl. Opt.*, *15*, 2085–2090, 1976.
- Rodgers, C. D., Some extensions and applications of the new random model for molecular band transmission, *Q. J. R. Meteorol. Soc.*, *94*, 99–102, 1968.
- Rodgers, C. D., and C. D. Walshaw, The computation of infrared cooling rate in planetary atmosphere, *Q. J. R. Meteorol. Soc.*, *92*, 67–92, 1966.
- Rothman, L. S., AFGL atmospheric absorption line parameters compilation: 1980 version, *Appl. Opt.*, *20*, 791–795, 1981.
- Rothman, L. S., R. R. Gamache, A. Barbe, A. Goldman, J. R. Gillis, L. R. Brown, R. A. Toth, J. M. Flaud, and C. Camy-Peyret, AFGL atmospheric absorption line parameters compilation: 1982 edition, *Appl. Opt.*, *22*, 2247–2256, 1983.
- Saiedy, F., Absolute measurements on infra-red radiation in the atmosphere, Ph.D. thesis, 43 pp., London Univ., 1960.
- Sasamori, T., The radiative cooling calculation for application to general circulation experiments, *J. Appl. Meteorol.*, *17*, 721–729, 1968.
- Schwarzkopf, M. D., and S. B. Fels, The simplified exchange method revisited: An accurate, rapid method for computation of infrared cooling rates and fluxes, *J. Geophys. Res.*, this issue.
- Stone, H. M., and S. Manabe, Comparison among various numerical models designed for computing infrared cooling, *Mon. Weather Rev.*, *96*, 735–741, 1968.
- Vigroux, F., Émission continue de l'atmosphère terrestre a 9.6 μ , *Ann. Geophys.*, *15*, 453–460, 1959.
- Washington, W. M., and G. A. Meehl, General circulation model experiments on the climatic effects due to a doubling and quadrupling of carbon dioxide concentration, *J. Geophys. Res.*, *88*, 6600–6610, 1983.
- Washington, W. M., and G. A. Meehl, Seasonal cycle experiment on the climate sensitivity due to a doubling of CO₂ with an atmospheric general circulation model coupled to a simple mixed-layer ocean model, *J. Geophys. Res.*, *89*, 9475–9503, 1984.
- Wetherald, R. T., and S. Manabe, Influence of seasonal variation upon the sensitivity of a model climate, *J. Geophys. Res.*, *86*, 1194–1204, 1981.

S. B. Fels and M. D. Schwarzkopf, Geophysical Fluid Dynamics Laboratory, NOAA, P. O. Box 308, Princeton University, Princeton, NJ 08542.

J. T. Kiehl, Climate Modeling Section, National Center for Atmospheric Research, P. O. Box 3000, Boulder, CO 80307.

A. A. Lacis, NASA Goddard Institute for Space Studies, 2880 Broadway, New York, NY 10025.

(Received July 3, 1990;
revised February 22, 1991;
accepted February 22, 1991.)